Journal of Civil Engineering
The Institution of Engineers, Bangladesh
Vol. CE 25, No. 1, 1997

ANALYSIS OF GROUND MOTIONS AT A RECLAIMED SITE DURING THE 1995 GREAT HANSHIN EARTHQUAKE

M. A. Ansary[1] F. Yamazaki[2] and T. Katayama [2]

ABSTRACT : Earthquake response analyses were conducted at a Kobe Port Island site (a reclaimed land), where surface and three downhole ground motions were recorded during the 1995 Great Hanshin earthquake. These records were compared with the ground motion recorded at the Japan Meteorological Agency's Kobe station (a stiff soil site) which is located a few kilometers away. The analyses of the borehole records were conducted using a nonlinear dynamic effective stress method that takes into account the liquefaction under multi-directional shearing. The input motions were recorded directly at the base by the vertical array system. Computed and recorded ground motions and associated response spectra were found to be in good agreement. Coupled effects of two horizontal motions on the dynamic response and liquefaction of the ground were also examined.

KEY WORDS: Hanshin earthquake, effective stress analysis, liquefaction, multi-spring model.

INTRODUCTION

The Great Hanshin earthquake on January 17, liquefied many sites in the Kansai area. Most of the liquefaction occurred under the level ground condition (Ishihara, 1993). Liqueafaction phenomena were observed during many previous big earthquakes such as the 1989 Loma Prieta eathquake, the 1993 Kushiro-Oki earthquake. However, only very few of them have real-time earthquake recording just beneath a liquefied site. So far, laboratory experiments on soil liquefaction (Erten and Maher, 1995; Vucetic and Dobry, 1988) have provided valuable insight into the mechanisms associated with excess pore pressure buildup. However, there remains a need to identify and understand the in-situ characteristics of soil strength and stiffness degradation due to liquefaction during seismic excitation.

Most studies on seismic responses and liquefaction of level ground in the past consider only one horizontal component of ground shaking (Dikmen and Ghaboussi, 1984; Finn et al., 1977; IShihara and Towhata, 1980; Martin an Seed, 1979)(Usually, the horizontally layered ground is modelled as a one-dimensional system that propagates the horizontal base acceleration as a shear wave in the vertical direction. In actual case, the level ground is simultaneously subjected to three components of shaking. Many researchers (Ishihara and Nagasse, 1988. Seed et al.,

1 Department of Civil Engineering, BUET, Dhaka-1000, Bangladesh
2 Institute of Industrial Science, University of Tokyo, 7-22-1 Roppongi, Minato-ku, Tokyo-106, Japan

1978; Yamada and Ishihara, 1983; Yamazaki and Ishihara, 1980) have shown that liquefaction is more liable to occur under multi-directional loading than under uni-directional loading and that the effective stress method is more suitable than the total stress method to take into account the time-dependent stiffness degrading effect caused by the pore pressure buildup in the soil (Ishihara and Towhata, 1980). In this study the authors used multi-spring model (Towhata and Ishihara, 1985; Yamazaki et al., 1985) for effective stress dynamic response analysis of a liquefied site at the Kobe port area.

CONSTRUCTION, LOCATION AND SITE CONDITION OF PORT ISLAND

Port Island is situated in Osaka Bay, south of Kobe city as shown in Figure 1 (a). The first stage of Port Island which has an area of 436 ha was completed in 1981. In the south, the second stage of Port Island with an area of 390 ha is originally planned to be completed in 1996. The island was built by placing granular fills (decomposed granite) on top of soft clay at the seabed (Tanaka, 1995). The water level in Kobe port varies from 15 to 20m approximately, and the fill level of the island was 4 to 5m above sea level. The shore line to the island was protected by a line of concrete caissons. These caissons were placed on top of sand and gravel fills that replaced the superficial soft marine clay layer after dredging.

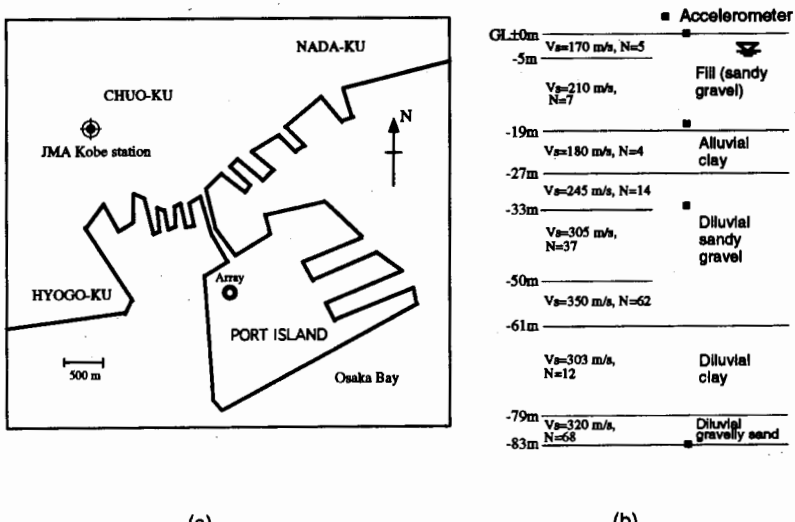

Fig 1. Location of Port Island array and JMA station in Kobe and (b) soil condition at the site

During the Great Hanshin earthquake, extensive liquefaction of ground and large lateral movements of concrete caissons were observed in Port Island. Settlement of ground due to the liquefaction was estimated to be 5 to 60 cm in Port Island (Erten and Maher, 1995). Figure 2 shows a typical liquefied site in Port Island.

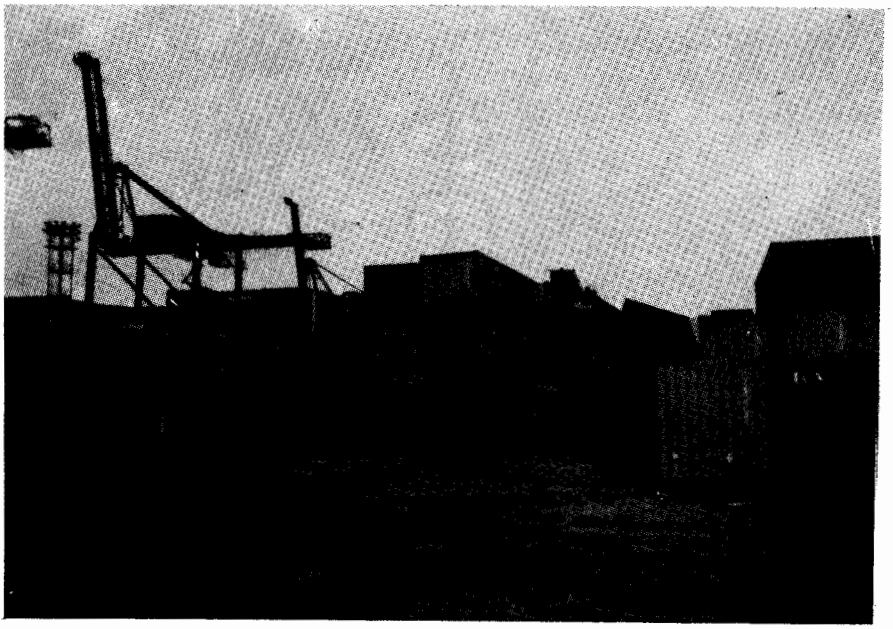

Fig 2. Liquefaction of a container yard at Port Island

The seismic motions of the reclaimed lands were monitored at Port Island by a one-dimensional vertical array. It is located at 34.670° north and 135.208° east at the northwestern part of the island and is shown in Figure 1 (a). The array consists of 4 three-component accelerometers at different depths of the borehole, namely at the ground surface (GL±0m), GL-16m, GL-32m and GL-83m. The soil condition at the site is shown in Figure 1(b). From the borehole report, it can be summarized that up to a depth of 19m is covered by fill, it is followed by an alluvial clay deposit from 19 to 27m. Next there is diluvial soil layer composed of gravelly sand from 27 to 61m, which is followed by a diluvial clay layer from 61 to 79m. Below the clay layer there exists a gravelly sand layer. The water table is situated approximately at a depth of 4m from the ground surface.

In this array site, orientation errors were detected from particle orbit plots of two horizontal components and were estimated by applying the maximum coherence method and the maximum cross-correlation method (Yamazaki et al., 1992). The ground surface at this site was supposed to be liquefied, so the accelerometer at GL-32m was used as the reference point instead of the accelerometer at GL±0m. The orientation angles were determined with respect to the NS-EW coordinate system. The notations and the positive directions of the coordinate axes and the angles are shown in Figure 3. In the orientation error analysis, β and γ angles were assumed to be zero. It was found from the main shock and the two aftershock records at hand that, with respect to the reference point accelerometers at GL±0m and GL-16m may not have any relative

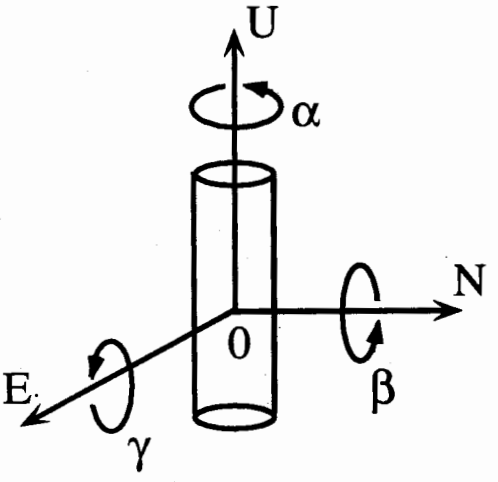

Fig 3. Coordinate system and orientation angles

orientation error, whereas the accelerometer at GL-83m may have a relative orientation error of 19° for α. Figure 4 shows Lissajous figures formed by the two horizontal components at two depths, before and after rotation for the main shock records. For further analysis of this study, corrected records were used.

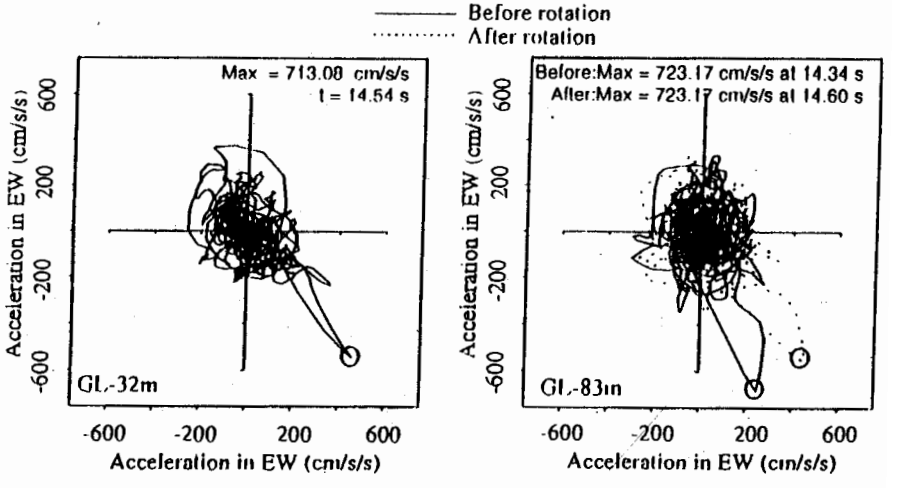

Fig 4. Lissajous figures at two depths of the array

RECORDED GROUND MOTIONS AT JMA KOBE STATION AND PORT ISLAND

To have a general view about the site effects and ground amplification, the authors considered two sites of different soil conditions. The first site is JMA's (Japan Meteorological Agency) Kobe station, which is a stiff soil site and the second is the site under investigation. The distance between these two sites is approximately 3 kilometers.

Figure 5 compares the response spectra between the sites. The Kobe Port Island Array (KPIA) site has a longer-period motion than that of the

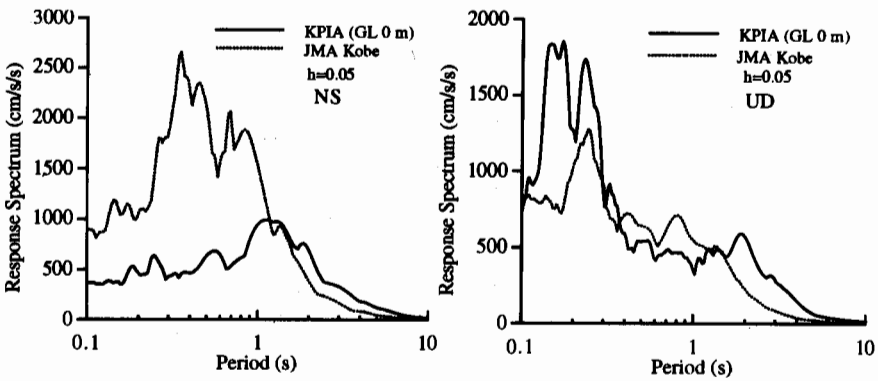

Fig 5. Comparison of acceleration response spectra of the JMA Kobe station and Port

JMA Kobe station for NS component. For the UD component, the sites have similar period content. The significant long period motion may be attributed to the occurrence of liquefaction in the reclaimed site. To investigate further, Figure 6 compares the response spectra for all the recorded NS and UD components of the vertical array system. For the NS component, except for the GL±0m record, the other three records have almost the same period contents. Also, the amplitudes of the spectra do not change much with the depth. Although not shown in the figure, for the EW component, the GL±0 record shows longer period but amplitudes for the four depths are almost the same. For UD component, liquefaction has almost no effect. The period contents for the peaks of those 4 records are within a very narrow band and spectral amplitude increases with decreasing depth.

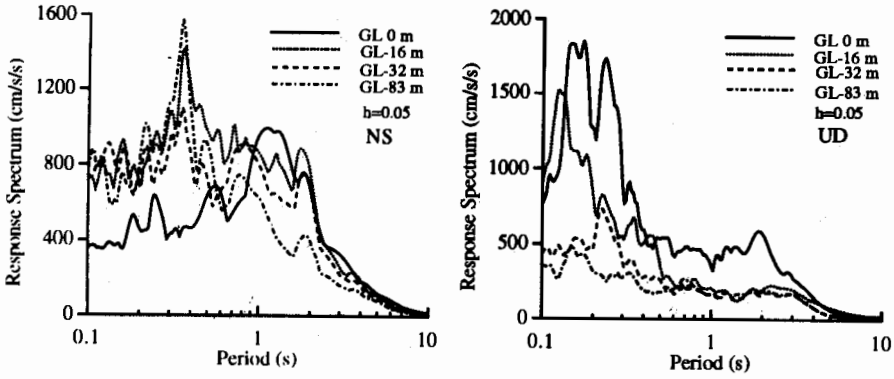

Fig 6. Comparison of acceleration response spectra of different depths of Port Island

MULTI-SHEARING MODEL AND SOIL PARAMETERS

The effective stress model used in this study was proposed by Yamazaki et. al (1985). It is composed of both deformation model with multiple nonlinear springs and pore pressure model based on a strain energy concept.

The stress-strain model called the multi-spring model consists of two rigid rings and numerous nonlinear springs connected as shown in Figure 7. When it represents a soil element, external forces are applied to the inner ring while the outer ring is fixed. Relation between force and deformation of each spring follows the modified Ramberg-Osgood model with Masing rule as proposed by Ohsaki et al. (1978). For pore pressure model, it was assumed that excess pore water pressure is determined solely by accumulated shear strain energy and current values of shear stress of a soil element.

In the absence of any experimental data for the site under study, the pore pressure parameters were determined using the experimental results of Toyura sand. Initial shear modulus for different soil layers was obtained from PS-logging and ϕ' values from a SPT N-ϕ' relation. It was assumed that there would be no pore pressure rise for clay layers. For sand and gravel layers, pore pressure parameters a and r were determined by using the relations between shear strain energy (W_S) and pore water pressure at zero shear stress (u_O) for different relative densities suggested by Towhata and Ishihara (1985). The values of W_S and u_O obtained for a particular relative densities were normalized by initial effective stress (σ'_{zo}) and substituted in the empirical relations suggested by Yamazaki et al. (1985) to obtain parameters a and r. The empirical relations are shown below :

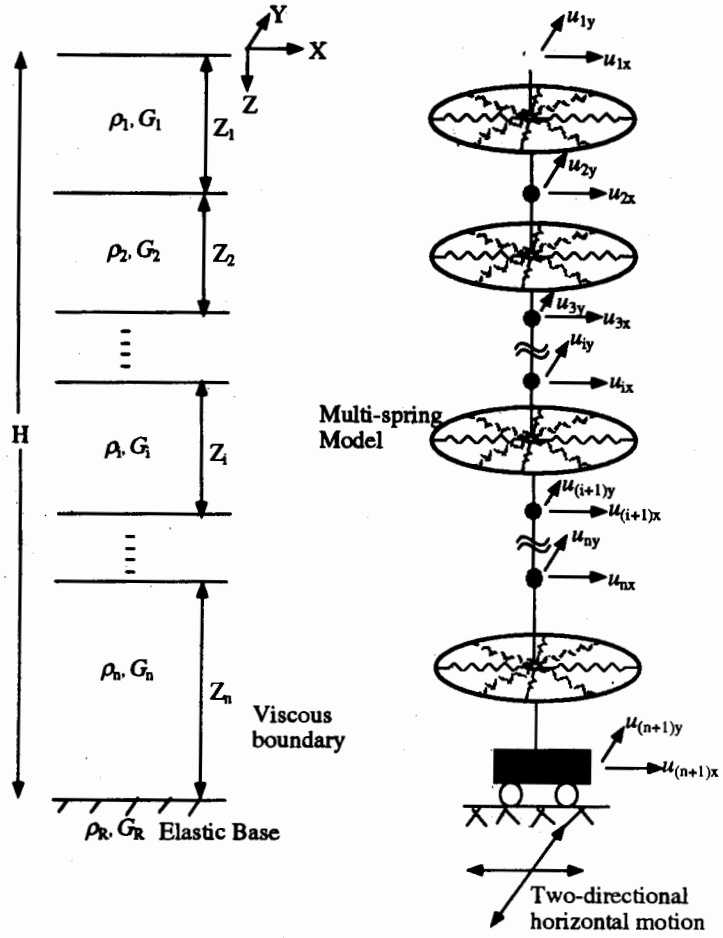

Fig 7. Model for dynamic response analysis in two-directional horizontal motion

$$\frac{u_o}{\sigma'_{zo}} = 1/(1+(r/(W_S / \sigma'_{zo}))^a); \text{ when } u_o/\sigma'_{zo} \leq 0.5 \quad (1)$$

$$\frac{u_o}{\sigma'_{zo}} = \frac{a}{4}(\ln(W_S / \sigma'_{zo}) - \ln r) + 0.5; \text{ when } 0.5 < u_o/\sigma'_{zo} \leq 1.0 \quad (2)$$

The relative density, D_r, for different sands were obtained using the Meyerhof (1957) empirical relation,

$$D_r = 21\sqrt{N/(\sigma'_V + 0.7)} \quad (3)$$

where σ_V' is the effective overburden pressure in kgf/cm^2. The soil parameters used for this study are shown in Table 1. Here, failure strain was taken as 3% and damping ratio as 0.35 as suggested by Ishihara

(1982) for large strain. Similar to clay layers, it was assumed that no pore pressure would be generated, for some deep soil layers. The permeability of clay layers is assumed as 10^{-8} m/s; of sand, 10^{-3} m/s; and of gravel, 10^{-2} m/s. C_r, the correction factor of failure strains between the single spring and the multi-spring, was determined from liquefaction analysis on a single soil element to be 0.80 for the Ramberg-Osgood model. Cp, a pore pressure parameter, was determined from laboratory tests to be 0.05.

To carry out the integration with respect to the depth, the soil layers were divided into a number of sublayers. These sublayers were converted into a lump-mass system as shown in Figure 7 in which the masses are connected by the multi-spring model.

Table 1. Soil properties used for the analysis of Port Island array

Layer No.	Thick-ness (m)	ρ_t (g/cm^3)	Porosi-ty n	K_o value	$G_t \cdot 10^3$ (KN/m^2)	$m_v \cdot 10^{-3}$ (m^2/t)	ϕ' (degree)	a'	r $\cdot 10^{-3}$
1	2.0	1.85	0.60	0.5	53.46	-	33.0	-	-
2	2.0	1.85	0.60	0.5	53.46	-	33.0	-	-
3	2.0	1.85	0.60	0.5	81.59	1.80	34.0	0.818	2.03
4	2.0	1.85	0.60	0.5	81.59	1.80	34.0	0.818	2.03
5	2.0	1.85	0.60	0.5	81.59	1.80	34.0	0.818	2.03
6	2.6	1.85	0.60	0.5	81.59	1.80	34.0	0.818	2.03
7	1.4	1.95	0.60	0.5	86.00	1.80	34.0	0.818	2.03
8	2.0	1.95	0.60	0.5	86.00	1.80	34.0	0.818	2.03
9	3.0	1.95	0.60	0.5	86.00	1.80	34.0	0.818	2.03
10	2.0	1.65	0.40	0.5	53.46	6.00	31.5	1.000	∞
11	2.0	1.65	0.40	0.5	53.46	6.00	31.5	1.000	∞
12	2.0	1.65	0.40	0.5	53.46	6.00	31.5	1.000	∞
13	2.0	1.65	0.40	0.5	53.46	6.00	31.5	1.000	∞
14	1.0	1.95	0.35	0.6	117.05	0.90	38.0	0.818	2.03
15	2.0	1.95	0.35	0.6	117.05	0.90	38.0	0.818	2.03
16	2.0	1.95	0.35	0.6	117.05	0.90	38.0	0.818	2.03
17	1.0	1.95	0.35	0.6	117.05	0.90	38.0	0.818	2.03
18	4.0	1.95	0.35	0.6	181.40	0.90	46.0	0.715	2.73
19	4.0	1.95	0.35	0.6	181.40	0.90	46.0	0.715	2.73
20	4.0	1.95	0.35	0.6	181.40	0.90	46.0	1.000	∞
21	4.0	1.95	0.35	0.6	181.40	0.90	46.0	1.000	∞
22	4.0	2.00	0.35	0.6	245.00	0.90	48.0	1.000	∞
23	4.0	2.00	0.35	0.6	245.00	0.90	48.0	1.000	∞
24	4.0	2.00	0.35	0.6	245.00	0.90	48.0	1.000	∞
25	6.0	1.95	0.30	0.7	179.30	0.75	46.0	1.000	∞
26	6.0	1.95	0.30	0.7	179.30	0.75	46.0	1.000	∞
27	6.0	1.95	0.30	0.7	179.30	0.75	46.0	1.000	∞
28	4.0	2.00	0.30	0.7	204.80	0.90	52.0	1.000	∞

Definition of the symbols used in the table :

a and r are pore pressure parameters determined by laboratory tests, ρ_t is the soil density, Ko is the coefficient of earth pressure at rest, G_t is the initial shear modulus m_v is the coefficient of volume compressibility and ϕ' is the angle of internal friction.

ANALYSIS OF THE SITE

Dynamic response analysis using effective stress method and multi-directional shearing for soil element was first applied for Kawagishi-cho site (45 km from the epicenter) during the 1964 earthquake in Nigata (Yamazaki et al., 1985). For the analysis of that site there was no appropriate input motion. The acceleration records obtained at the basement of a building located on a stiff soil site in Akita City (180 km from the epicenter) during the earthquake were rescaled to have appropriate predominant period and maximum amplitude, and were used as incident waves at the base layer. The site also contained almost uniform soil, i.e., medium to fine sand. On the other hand, for the site under consideration, the acceleration records were obtained at several depths. The site contains some deep clay layers interspersed with sandy gravel layers which might have caused liquefaction at some deep layers. Based on these facts, this may be a good opportunity to check the effectiveness of multi-shearing model for simulating liquefaction at this site.

The acceleration records obtained in the GL-83m in the vertical array was directly used as the incident waves. The maximum amplitudes were 560.5 cm/s^2 in the NS direction and 456.9 cm/s^2 in the EW direction. Dynamic effective stress analyses in two-directional motion and in uni-directional motion were conducted.

In general, the agreement between computed and observed results is fairly good, whereas a little discrepancy in peak heights and shift of peak locations appear in some part of the time histories. Figures 8 and 9 show recorded motion at the base level (GL-83m) and comparison between recorded motion and calculated motion on the ground surface for both two-directional and uni-directional input motions. In these figures, ground motions from 10 to 35s are presented. The agreement appears to be very good in the region of strong shaking, and the computed post-liquefaction responses after 16s are somewhat weaker than the recorded motions. This may be due to the fact that the residual stiffness and stiffness and strength assumed for the post liquefied soil is too soft. Other factors that may contribute to the discrepancy between recorded and computed motions may arise from the nature of the ground motions and the assumptions used in the 1D-analysis.

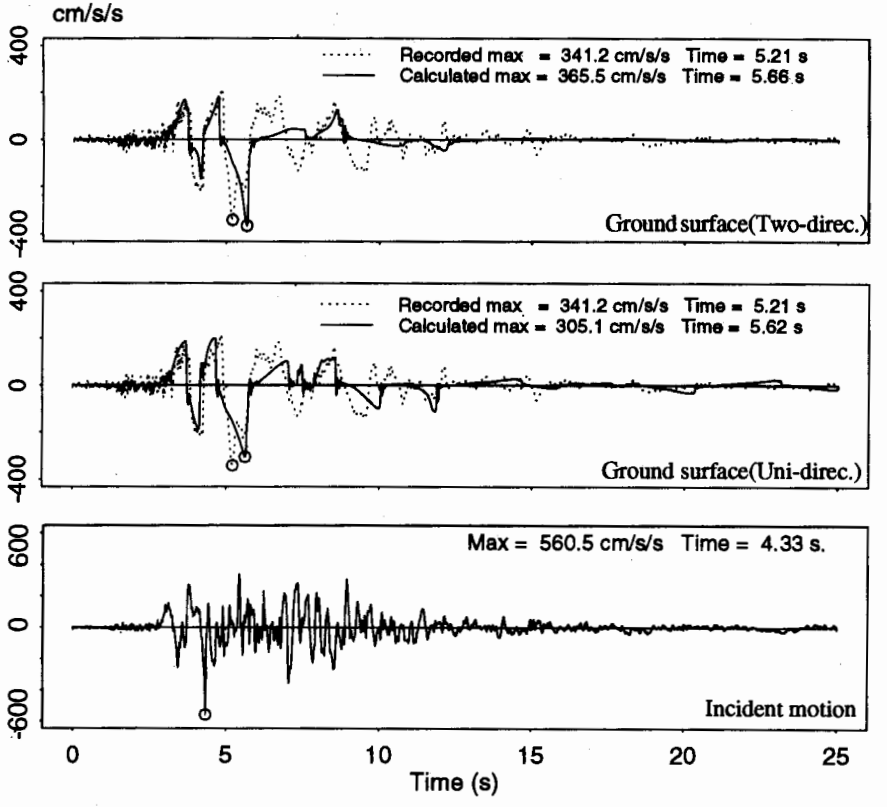

Fig 8. Computed acceleration time histories by uni-directional and two-directional analysis for the NS component

Figure 10 shows the computed and observed acceleration response spectra of the ground surface for the NS and EW components. It can be seen that the predominant periods for the observed and the computed spectra are the same although the amplitudes on the peaks are not equal. For the longer period range, spectrum values are higher for the uni-directional analysis compared with the two-directional analysis. Such effects may be attributed to the fact that non-linearities of the loose layer were intensified by the combined motion. Figure 11 shows the distribution of the computed maximum accelerations for the NS and EW components together with the recorded values. For top soil layers up to a depth of 16m, maximum accelerations by two-directional analysis are larger than those by uni-directional analysis for the NS and EW components. For depths below 16m, the accelerations obtained by both analyses are the same for the NS component and the accelerations

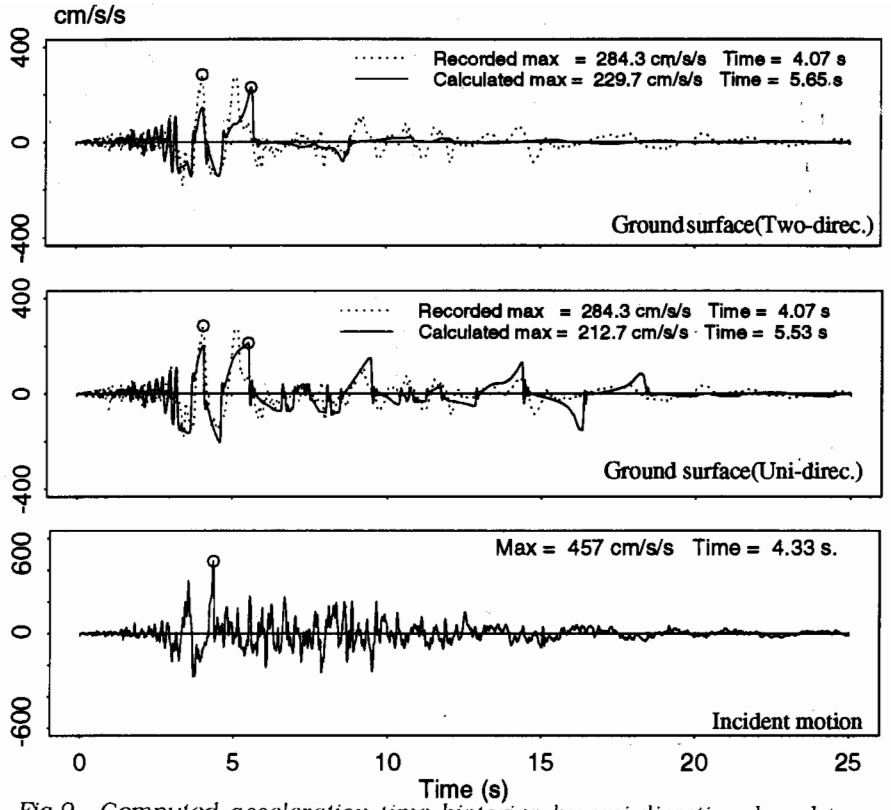

Fig 9. Computed acceleration time histories by uni-directional and two-directional analysis for the EW component

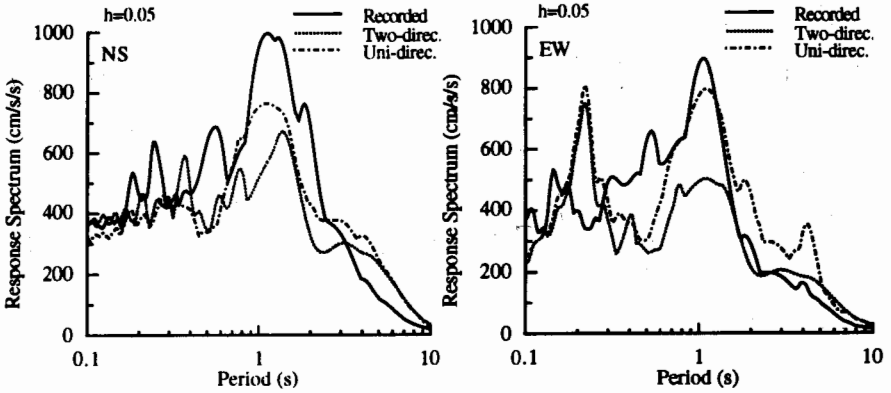

Fig 10. Computed and observed acceleration response spectra of the ground surface for the NS and EW components

obtained by the uni-directional analysis are comparatively larger than those by the two-directional analysis for the EW component. In this preliminary stage of the analysis, the reasons for such change of responses with depth are not clear, but liquefaction of the top soil layers may be the cause.

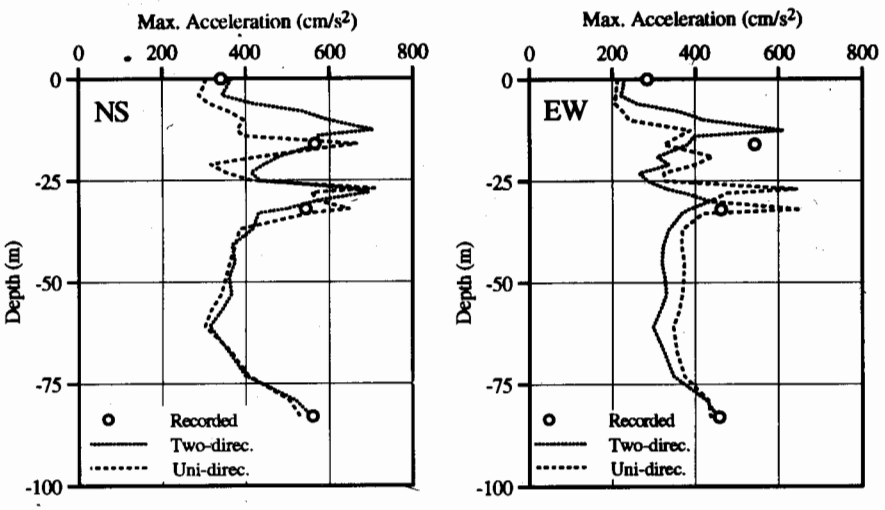

Fig 11. Distribution of the computed maximum acceleration for the NS and EW components

Figure 12 which show the variation of maximum shear strain with depth indicates possible liquefied layers, where the maximum strains exceed the specified failure strain. Figure 13 which shows maximum excess pore water pressure variation with depth also indicates the liquefied layers where initial effective vertical stress equals excess pore water pressure.

Liquefaction may occur in more than one layer and at different times. In the two-directional analysis, liquefaction occurred in the loose layer at GL-10m to 16m (i.e., layers #6 to #8) and at GL-27m to - 33m (layers#14 to #17). In the uni-directional analysis, liquefaction occurred only in the loose layer at GL-10m to - 16m. For the two-directional analysis, liquefaction might have started at both depths simultaneously but complete liquefaction might have occurred first in the lower level and later in the upper level. It is generally thought that liquefaction can not occur below a depth of 20m , but in this case liquefaction in the lower level may be due to the very strong ground motion in an intermediate soft layer. On the other hand, liquefaction in the upper layers can be explained by the fact that liquefaction may also occur due to the seepage forces exerted by the upward flow of water as the pore-water pressures

remaining in the soil will try to dissipate in the vertical direction. Generally, this type of liquefaction occurs near the ground surface.

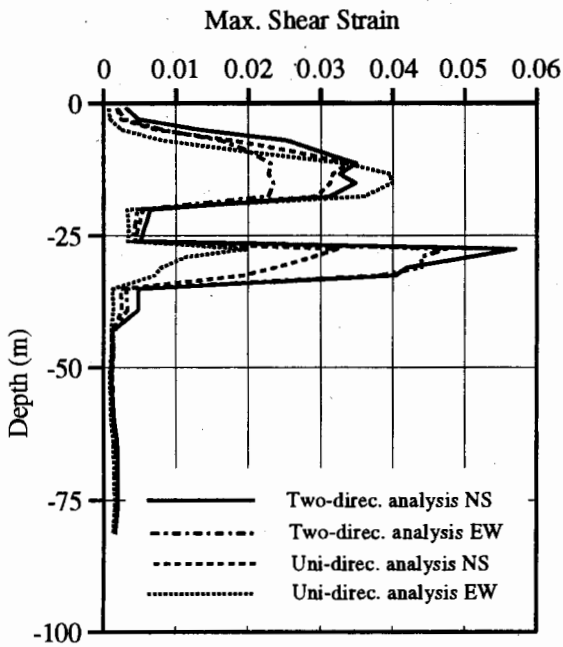

Fig 12. Distribution of the computed maximum shear strain

In the uni-directional analysis, the maximum pore-water pressures developed in layer #6 were 98% of the initial effective vertical stress by both the NS and EW motions. For layer #14, maximum pore water pressures developed were 93% and 98% of the initial effective vertical stress by NS and EW-motions respectively. Figure 14 shows the computed time histories of pore-water pressures in two liquefied layers.

Figure 15 shows the variation of G/G_O and h with depth. In this figure, it is clear that at the liquefied layers, soil stiffness becomes low and damping ratio becomes large. Liquefaction is generally accompanied by large strain. At large strain condition, soil stiffness reduces and damping ration increases. Figure 15 also shows that the combined two-directional motion hastens the soil stiffness degradation more than the uni-directional ground motion due to high nonlinear behavior.

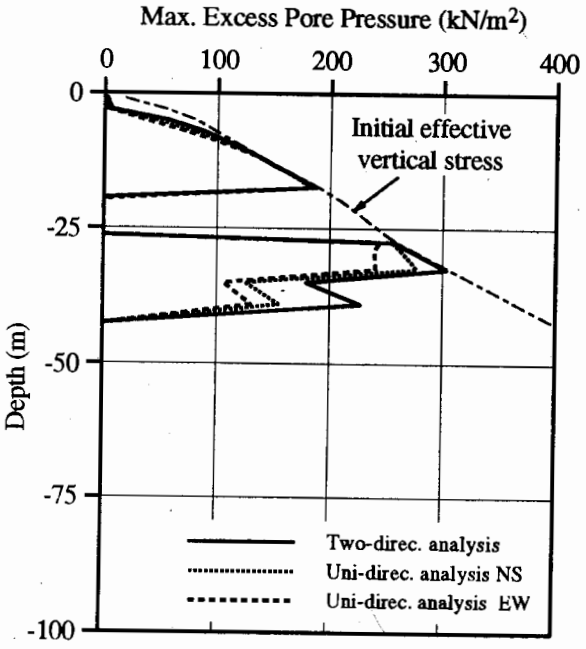

Fig 13. Distribution of the computed maximum excess pore water pressure

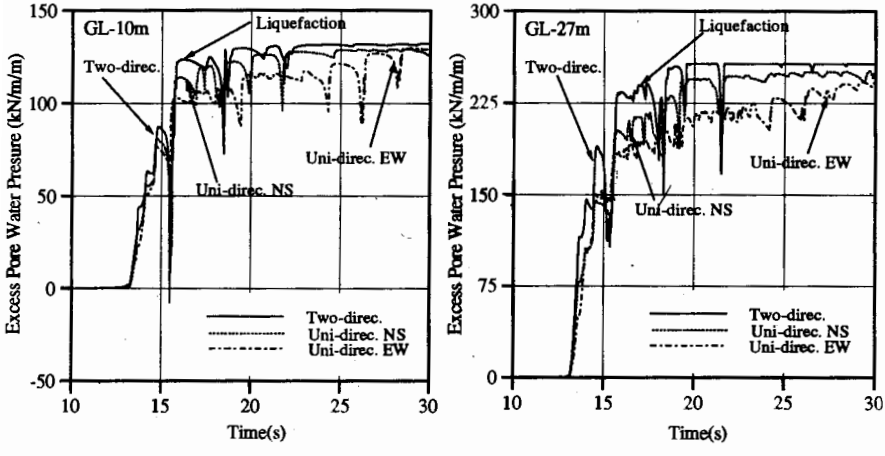

Fig 14. Computed time histories of pore-water pressures in the two liquefied layers

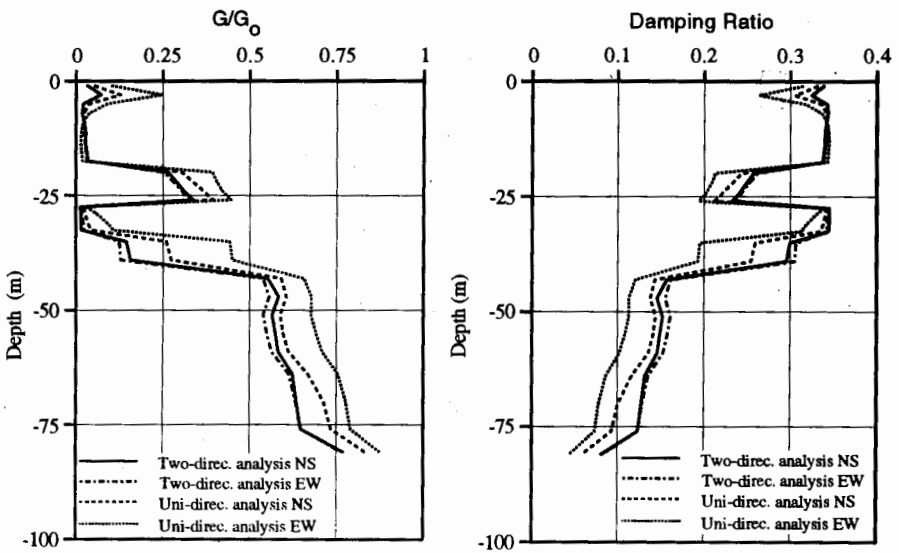

Fig 15. Variation of G/Go (left) and damping ratio (right) with depth

CONCLUSIONS

From the acceleration response spectra of ground motion at Kobe JMA station and Port Island site, it can be observed that amplitudes of the horizontal spectral components are higher and the period is longer at the Port Island site than those at the JMA site. The longer period of liquefied ground resulted from the softening of the site by strong earthquake shaking.

Using the main shock and two relatively smaller aftershock records at hand the authors detected an orientation error in the deepest point of the vertical array. Further analysis should be made with several earthquake events to establish this point.

In this study, a dynamic effective stress method composed of multi-directional shearing model was used for liquefaction simulation at the site. Results of this analysis show that the combined two-directional input motion is more liable to cause liquefaction but induces smaller acceleration response spectrum than the uni-directional input motion. This may be attributed to the intensification of the non-linearities by the combined motion.

For this particular site, along with the liquefaction at a shallow depth, liquefaction was also detected in a deep layer. The reason may be due to the presence of a soft intermediate layer and specially strong ground motion.

ACKNOWLEDGEMENT

The authors would like to thank the Committee of Earthquake Observation and Research in the Kansai Area (CEORKA) for providing him with the earthquake records at the Port Island site.

REFERENCES

Dikmen, S.U. & Ghaboussi, J. (1984). Effective stress analysis of seismic response and liquefaction : Theory, J. Geotech. Engg. Div., ASCE **110(GTS)**: 628-644.

Erten, D. & Maher, M. H. (1995). Cyclic undrained behavior of silty sand, *Soil Dyn. & Earthq. Engng.* **14**: 115-123.

Finn, W.D.L., Lee, K.W. & Martin, G.R. (1977). An effective stress model for liquefaction, *J. Geotech. Engg. Div., ASCE* **103(GT6)**: 517-533.

Ishihara, K. & Towhata, I. (1980). One-dimensional soil response analysis during earthquakes based on effective stress method, *J. of the Faculty of Engg.*, University of Tokyo (B) **XXXV(4)**: 655-700.

Ishihara, K. (1982). Evaluation of soil properties for use in earthquake response analysis, *Int. Symp. on Numerical Methods in Geomechanics, Zurich*, pp. 237-59.

Ishihara, K. & Nagase, H. (1988). Multi-directional irregular loading tests on sand, *Soil Dyn. & Earthq. Engng.* **7**: 201-212.

Ishihara, K. (1993). Liquefaction and flow failure during earthquakes, *Geotechnique* **43(3)**: 351-415.

Martin, P.P., Seed, H. B. (1979). Simlified procedure for effective stress analysis of ground motion, *J. Geotech. Engg. Div., ASCE* **105(GT6)**: 739-758.

Meyerhof, G. G. (1957) Discussion, Proc. *4th Int. Conf. on Soil Mechanics & Foundation Eng.*, **3**: 110.

Ohsaki, Y., Hara, A. & Kiyota, Y. (1978). Stress-strain model of soils for seismic analysis, *Proc. of 5th Japan Earth Eng. Symp.*, pp. 697-703 (Japanese).

Seed, H.B., Pyke, R.M. & Martin, G.R. (1978). Effect of multi-directional shaking on pore pressure development in sands, *J. Geotech. Engg. Div. ASCE* **104(GT1)**: 27-44.

Tanaka, Y. (1995). Liquefaction and damage to harbour facilities, *2nd Report on Great Hanshin Earthquake*, Field Investigation Team on Great Hanshin Earthquake, Dept. of Civil Eng., Faculty of Eng., Kobe University, pp. 228-232.

Towhata, I. & Ishihara, K. (1985). Shear work and pore water pressure in undrained shear, *Soils & Foundations* **25(3)**: 73-84.

Towhata, I. & Ishihara, K. (1985). Modelling soil behavior under principal axes rotation, *Proc. 5th Int. Conf. on Numerical Methods in Geomechanics*, Nagoya, pp. 523-530.

Vucetic, M. & Dobry, R. (1988). Cyclic tiaxial strain controlled testing of liquefiable sands, *Advanced Triaxial Testing of Soil & Rock*, ASTM STP 977, *ASTM*, Philadelphia, Pa., pp. 475-485.

Yamada, Y. & Ishihara, K. (1983). Undrained deformation characteistics of sand in multi-directional shear, *Soils & Foundations* **23(1):** 61-79.

Yamazaki, F & Ishihara, K. (1980). Cyclic simple shear tests on saturated sand in multi-directional loading, *Soils & Foundations* **20(1):** 45-69.

Yamazaki, F., Towhata, I & Ishihara, K. (1985). Numeical model for liquefaction problem under multi-directional shearing on horizontal plane, *Proc. 5th Int. Conf. on Numerical Methods in Geomechanics*, Nagoya, pp. 399-406.

Yamazaki, F. Lu., L & Katayama, T. (1992). Orientation error estimation of buried seismographs in array observation, *Earth. Eng. Struct. Dyn.* **21**: 679-694.